A&A, 704, A256 (2025)
https://doi.org/10.1051/0004-6361/202554354

Astronomy & Astrophysics

Cluster Ages to Reconstruct the Milky Way Assembly (CARMA)

III. NGC 288 as the first Splashed globular cluster

E. Ceccarelli[1,2,⋆], D. Massari[1], F. Aguado-Agelet[3,4], A. Mucciarelli[2,1], S. Cassisi[5,6], M. Monelli[5,7], E. Pancino[8], M. Salaris[9], and S. Saracino[8,9]

[1] INAF – Osservatorio di Astrofisica e Scienza dello Spazio di Bologna, Via Gobetti 93/3, 40129 Bologna, Italy
[2] Dipartimento di Fisica e Astronomia, Università degli Studi di Bologna, Via Gobetti 93/2, 40129 Bologna, Italy
[3] atlanTTic, Universidade de Vigo, Escola de Enxeñaría de Telecomunicación, 36310 Vigo, Spain
[4] Universidad de La Laguna, Avda. Astrofísico Fco. Sánchez, 38205 La Laguna, Tenerife, Spain
[5] INAF – Osservatorio Astronomico di Abruzzo, Via M. Maggini, 64100 Teramo, Italy
[6] INFN – Sezione di Pisa, Università di Pisa, Largo Pontecorvo 3, 56127 Pisa, Italy
[7] INAF – Osservatorio Astronomico di Roma, Via Frascati 33, 00040 Monte Porzio Catone, Italy
[8] INAF – Osservatorio Astrofisico di Arcetri, Largo E. Fermi 5, 50125 Firenze, Italy
[9] Astrophysics Research Institute, Liverpool John Moores University, 146 Brownlow Hill, Liverpool L3 5RF, UK

Received 3 March 2025 / Accepted 21 July 2025

ABSTRACT

The system of globular clusters (GCs) in the Milky Way (MW) comprises a mixture of both in situ and accreted clusters. Tracing the origin of GCs provides invaluable insights into the formation history of the MW. However, reconciling diverse strands of evidence is often challenging. A notable example is NGC 288, where despite significant efforts in the literature, the available chrono-chemodynamical data have yet to provide a definitive conclusion regarding its origin. On the one hand, all post-*Gaia* dynamical studies indicate an accreted origin for NGC 288, pointing towards its formation taking place in the *Gaia*-Sausage-Enceladus (GSE) dwarf galaxy. On the other hand, NGC 288 has been found to be 2.5 Gyr older than other GSE GCs at the same metallicity, suggesting a different (and possibly in situ) origin. In this work, we address the unresolved question on the origin of NGC 288 by analysing its chrono-chemical properties in an unprecedentedly homogeneous framework. First, we compared the location of NGC 288 in the age-metallicity plane with that of other two GCs at similar metallicity, namely, NGC 6218 and NGC 6362, whose chemodynamical properties unambiguously identify them as in situ. The age estimates obtained within the homogeneous framework of the CARMA collaboration show that the three clusters are coeval, reinforcing the contrast with the dynamical interpretation. Then, we derived the chemical composition of NGC 288 using UVES-FLAMES at VLT high-resolution spectroscopic archival data and compared the abundances with a sample of in situ and accreted clusters at similar metallicity. We found a consistency with the chemistry of in situ systems, especially in Si, Ti, Zn, and abundance ratios relative to Eu. To reconcile these results with its orbital properties, we propose a scenario where NGC 288 formed in the proto-disc of the MW and was then dynamically heated by the interaction with the GSE merger. This is a fate that resembles that of proto-disc stars undergoing the so-called Splash event. Therefore, NGC 288 demonstrates the importance of a homogeneous chrono-chemodynamical information in the interpretation of the origin of MW GCs.

Key words. stars: abundances – Galaxy: formation – globular clusters: general – globular clusters: individual: NGC288

1. Introduction

The Milky Way (MW) has undergone a process of hierarchical accretion of smaller galaxies to build up its mass, as predicted by the ΛCDM cosmological paradigm (White & Frenk 1991). The *Gaia* mission (Gaia Collaboration 2016, 2023) has enabled us to unveil the dynamical fossil record of those events that were hidden in the Galactic halo (Helmi 2020), such as the last major merger experienced by the MW, which occurred roughly 10 Gyr ago with the dwarf galaxy *Gaia*-Sausage-Enceladus (GSE, Belokurov et al. 2018; Helmi et al. 2018). As a result of this impactful merger, the pre-existing MW disc became kinematically hotter, with a large fraction of its stars having had their orbits altered towards higher eccentricity. This process is sometimes referred to as the Splash (Di Matteo et al. 2019; Gallart et al. 2019; Belokurov et al. 2020).

It has been well-established that the most massive among the ingested dwarf galaxies harbored their own system of globular clusters (GCs) that were accreted alongside their stars (Peñarrubia et al. 2009; Kruijssen et al. 2019; Bellazzini et al. 2020; Malhan et al. 2022). Thus, the study and characterization of GCs stand out as a powerful probe of the MW assembly processes. Dynamical information derived from the measurements of the *Gaia* mission has allowed us to reconstruct the origin of each individual MW GC (Massari et al. 2019; Forbes 2020; Callingham et al. 2022; Chen & Gnedin 2024). However, this is not sufficient to achieve good accuracy in the associations, as coherent dynamical substructures are neither pure nor complete (Pagnini et al. 2023; Chen & Gnedin 2024; Mori et al. 2024). Clues about the origin of GCs provided by their orbital properties can be significantly enriched by incorporating the information on the age. As extensively shown in the literature, GCs that formed in accreted dwarf galaxies exhibit distinct age-metallicity relations (AMRs), which distinguish them from the

⋆ Corresponding author: edoardo.ceccarelli3@unibo.it

trajectory followed by GCs formed in situ (Marín-Franch et al. 2009; Forbes & Bridges 2010; Dotter et al. 2010; Leaman et al. 2013; Massari et al. 2019), at least in the metal-intermediate and metal-rich regimes ([M/H] > -1.3 dex).

In this context, one peculiar case is that related to the GC NGC 288. In fact, the orbital properties of this cluster, which is located in the Halo at a distance of 9.0 kpc from us (Vasiliev & Baumgardt 2021), suggest an accreted origin from the GSE merger event (Massari et al. 2019; Forbes 2020; Callingham et al. 2022; Chen & Gnedin 2024). However, contrasting evidence has been found in the literature regarding its age. For example, several works found NGC 288 to be about 2 Gyr older than NGC 362 (i.e. a GSE GC with similar metallicity, Green & Norris 1990; Sarajedini & Demarque 1990; Bellazzini et al. 2001; Gontcharov et al. 2021), whereas other works have reported an age difference between the two GCs always smaller than 1 Gyr (Stetson et al. 1996; Dotter et al. 2010; VandenBerg et al. 2013). These inconsistencies might be caused by systematic effects due to different photometric systems, methods, and adopted theoretical models, that can easily add up to ∼2 Gyr (Massari et al. 2019). Further, several studies hint at differences in the chemical composition of NGC 288 compared to accreted GCs, especially regarding the α- (Horta et al. 2020) and the light elements (Belokurov & Kravtsov 2024), pointing towards a potential in situ formation. Also, Monty et al. (2023b) highlighted a poor agreement between NGC 288 and GSE field stars in the *s*- and *r*- process elements, showing that a chemical evolutionary model of a GSE-like galaxy fails to reproduce the abundances measured in NGC 288. However, also in these cases, the chemical evidence comes from spectra covering different spectral ranges analysed with different methods and from the adoption of different models, which might result in significant systematic errors.

In this work, we examine the chrono-chemodynamical profile of NGC 288, aiming to resolve the apparent contradictions arising from its peculiar properties. To do so, we compare age and chemical composition of NGC 288 with those of in situ MW GCs in the same metallicity range ([M/H] ~ -1.0 dex). The novelty of this study is that it is conducted within a completely homogeneous framework. On the one hand, GC ages are estimated by means of the tools developed within the Cluster Ages to Reconstruct the Milky Way Assembly (CARMA) collaboration (Massari et al. 2023, Aguado-Agelet et al. 2025, hereafter Paper I and II, respectively). On the other hand, the chemical analysis follows the same prescriptions and uses optical spectra obtained with the same instrument and with the same quality as in Ceccarelli et al. (2024, C24 hereafter). This kind of analysis erases any potential offset introduced by the use of different approaches, leading to an interpretation of the observational evidence with the utmost precision.

2. Comparison between the age of NGC 288 and in situ globular clusters

The first objective of this work is to compare the age of NGC 288 as found in Paper II with that of GCs at similar metallicity whose origin is clearly in situ. This type of relative comparison is, in fact, the best way to assess whether the hypothesis that NGC 288 is too old compared to GSE GCs to have been accreted is correct. According to the classifications by Massari et al. (2019) and Callingham et al. (2022), the only in situ disc GCs at [M/H] ~ -1.0 dex for which public Hubble Space Telescope (HST) photometry is available are NGC 6218 and NGC 6362. For both GCs, an in situ origin is supported by chemistry as well as by dynamics (Belokurov & Kravtsov 2024, C24).

To estimate the age of NGC 6218 and NGC 6362, we used photometry in the HST F606W and F814W filters from the HUGS survey (Piotto et al. 2015; Nardiello et al. 2018). In accordance with the typical prescriptions adopted by CARMA, we selected stars with a proper motion-based probability membership of >90% and we applied a differential reddening correction (Milone et al. 2012, see Appendix A.1 for details).

The isochrone fitting method employed to derive the age of NGC 6218 and NGC 6362 is presented in Paper I (see Appendix A.2 for a brief summary of the methodology). The results of the isochrone fitting in both optical CMDs for these GCs are shown in Figs. 1 and 2 and summarised in Table 1. In the top panels of each figure, we show the best-fit isochrone superimposed on the two CMDs. Grey points represent the stars selected according to the methods described above (see also Appendix A), while green points indicate stars specifically used for the fit. The posterior distributions of the parameters of the models are presented in bottom panels alongside the corner plot with the best fit values for [M/H], color excess, distance modulus, and age. To compare the global metallicity with literature results, we transformed [M/H] into the iron abundance following the prescriptions described in Paper II. Thus, the photometric solution derived in this work translates to [Fe/H] $= -1.38$ dex for NGC 6218 and [Fe/H] $= -1.08$ dex for NGC 6362, which is consistent within 0.1 dex with spectroscopic measurements (Carretta et al. 2009; Massari et al. 2017). The median color excess values are $E(B-V) = 0.20 \pm 0.01$ and $E(B-V) = 0.07 \pm 0.01$ for NGC 6218 and NGC 6362, respectively. This is also in agreement with previous literature estimates reported in Harris (2010). Also, the distance modulus is well recovered, with differences with values listed in the Harris (2010) catalogue up to 0.15 mag, but fully consistent with results from Baumgardt & Vasiliev (2021).

In Fig. 3, we present the AMR for the two GCs under study in this work (red filled squares) together with the results obtained for the metal-rich in situ GCs (red filled circles) in Paper I, the in situ cluster ESO452-11 (red filled triangle) from Massari et al. (2025), and the dynamically selected GSE GCs (green filled circles) in Paper II. As made evident by the figure, the age of NGC 288 is fully consistent within the uncertainties with that of the two in situ GCs analysed here. The mean age of the three GCs is 13.68 Gyr, with a very small dispersion of 0.19 Gyr. This in turn means that the three GCs are ∼2.5 Gyr older than the sample of GSE GCs at the same metallicity, as expected for clusters that formed in an environment characterised by a higher star formation efficiency, compared to a dwarf galaxy such as GSE (Kruijssen et al. 2019; Souza et al. 2024; González-Koda et al. 2025). All the collected evidence therefore supports the interpretation of NGC 288 as born in situ in the MW, in contrast to its orbital properties (Massari et al. 2019; Callingham et al. 2022). Finally, we note that one additional GSE system (i.e. NGC 6205, red empty circle) follows the same AMR as the three GCs described above, reinforcing the idea presented in Paper II, namely, that it is a contaminant in the fully dynamical selected GSE sample with a likely in situ origin. As this GC is more metal-poor than those analysed here, a comprehensive analysis of NGC 6205 is left to a future dedicated work.

3. The chemical composition of NGC 288

The combination of the chrono-dynamical information leads to contrasting results about the origin of NGC 288. In this

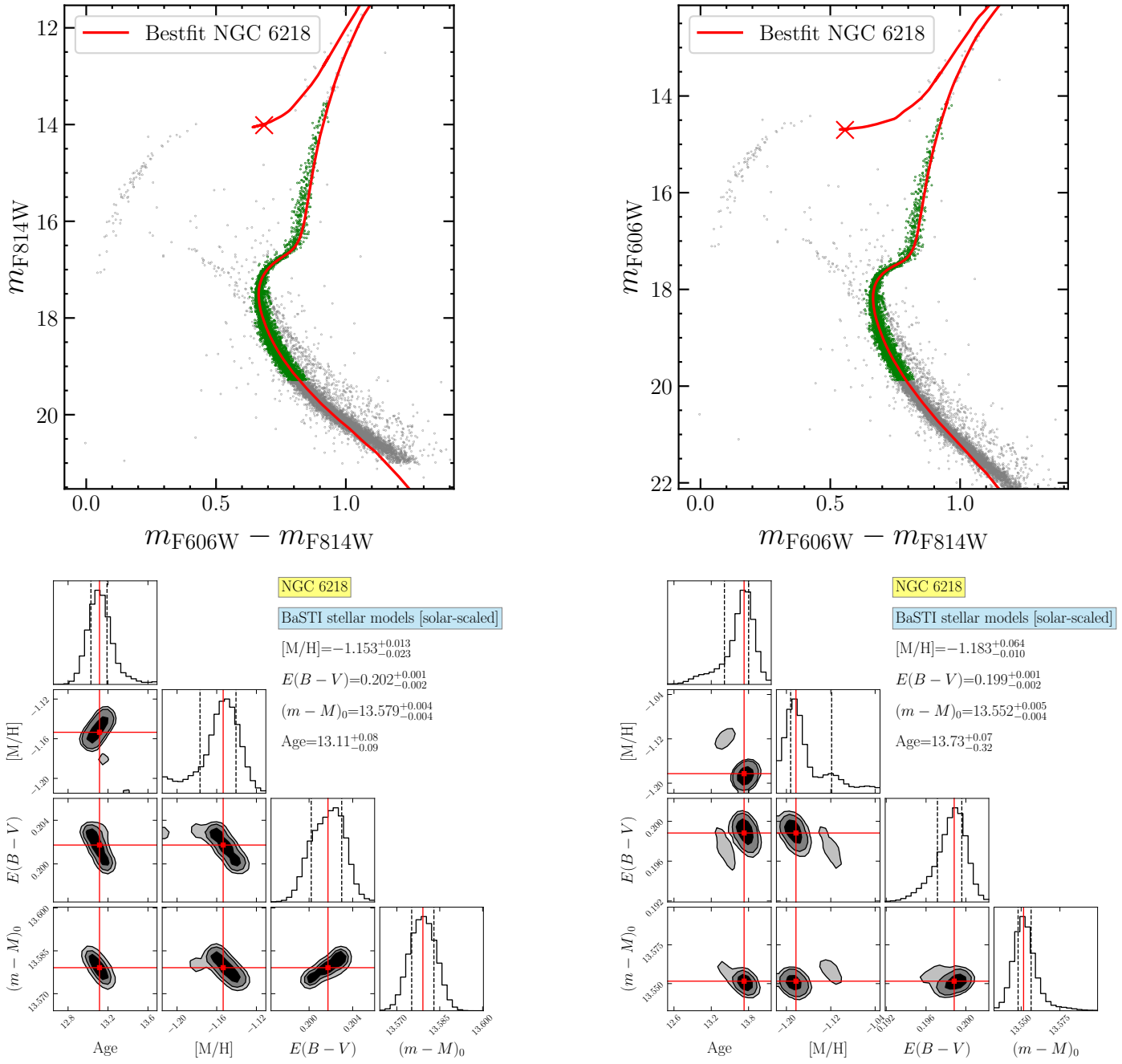

Fig. 1. Results for NGC 6218. Top-left: best-fit model in the (m_{F814W}, $m_{F606W} - m_{F814W}$) CMD. Top-right: best-fit model in the (m_{F606W}, $m_{F606W} - m_{F814W}$) CMD. Bottom-left: posterior distributions for the output parameters and the best-fit solution, quoted in the labels, in the (m_{F814W}, $m_{F606W} - m_{F814W}$) CMD. Bottom-right: posterior distributions for the output parameters and the best-fit solution, quoted in the labels, in the (m_{F606W}, $m_{F606W} - m_{F814W}$) CMD.

context, the chemical composition of this system can plays a crucial role, since the abundances of stars reflect the chemical enrichment history of the environment where they formed. Thus, a detailed study of the chemical makeup of this GC can favour one of the two scenarios described above, offering clues to finally solving the puzzle regarding its origins. To do so, we followed the same approach used for the chronological information: a relative, systematic-free comparison between the abundances of NGC 288 and that of in situ and accreted GCs (C24).

To perform the chemical analysis, we collected archival data of ten red giant branch (RGB) stars in NGC 288 that have been observed under the ESO-VLT Programme 073.D-0211 (PI: E. Carretta) using the multi-object spectrograph UVES-FLAMES (Pasquini et al. 2002) mounted at the Very Large Telescope. The spectra were acquired using the Red Arm 580 CD3 grating with a spectral coverage between 4800 and 6800 Å, along with a spectral resolution of R ∼ 40 000. The typical signal-to-noise ratio is S/N ≥ 55 at 6000 Å. The spectra were reduced using the dedicated ESO pipeline[1]. The sky background emission was measured by observing empty sky regions and subsequently subtracted from each single stellar spectrum. To ensure homogeneity in the spectroscopic analysis, we followed the same approach

[1] https://www.eso.org/sci/software/pipelines/

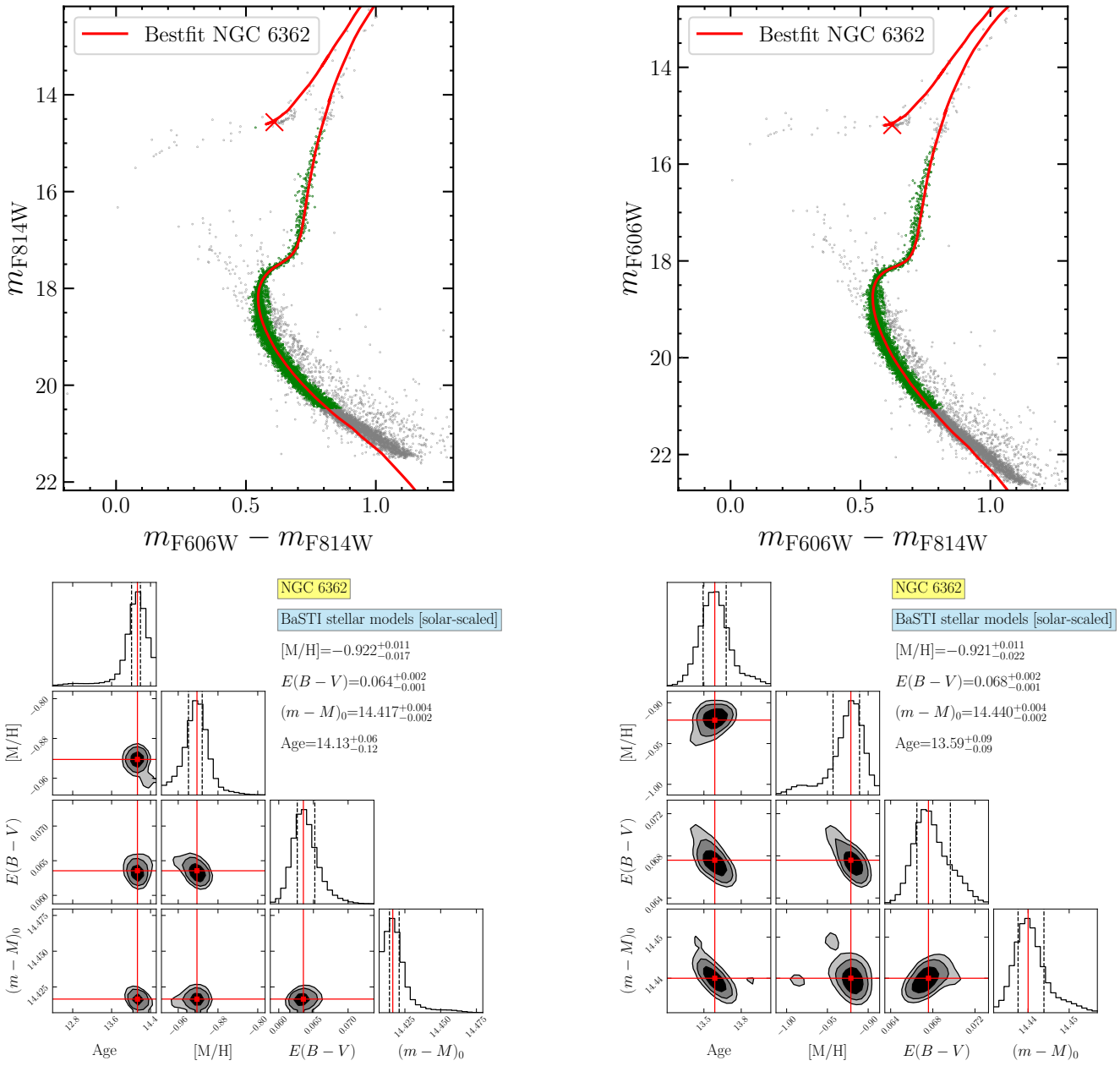

Fig. 2. Same as Fig. 1, but for NGC 6362.

used in C24 to derive the atmospheric parameters and elemental abundances of target stars. For details of the chemical analysis, we refer to C24 and references therein. A concise summary can be found in Appendix B. The mean abundances for NGC 288 for key chemical elements that have proven their efficiency in disentangling accreted and in situ formation (i.e. α-elements, Zn, Eu, C24) are listed in Table 2. The abundances of single stars can be found in Tables B.2 and B.3. The average iron content derived from neutral iron lines is [Fe/H] $= -1.21 \pm 0.01$ dex, in good agreement with either spectroscopic (Carretta et al. 2009; Horta et al. 2020) and photometric solutions (see Paper II).

In Fig. 4, we compare the average abundance of NGC 288 (blue symbol) and several MW GCs from C24, distinguishing between in situ (NGC 6218, NGC 6522 and NGC 6626, red symbols) and accreted from GSE (NGC 362 and NGC 1261, green symbols). As illustrated in the left panel, NGC 288 consistently shows enhancement (≥0.1 dex) in α-elements Si and Ti, compared to GSE GCs, with values comparable to those found in in situ GCs. A similar enhancement is also observed in Mg. Moreover, the average [Zn/Fe] ratio in NGC 288 is consistent (within the uncertainties) with that of in situ GCs. Given that absolute values of abundance ratios across different inhomogeneous studies may be subject to systematic zero-point offsets, our comparisons with literature are based on relative abundance differences derived within homogeneous analyses. The α-element enhancements we find for NGC 288 relative to the GSE GC NGC 362 are consistent with results from previous studies (Shetrone & Keane 2000; Carretta et al. 2009; Carretta et al. 2010, 2013; Horta et al. 2020; Monty et al. 2023a,b, see also the discussion in the appendix of C24). Additionally, Monty et al. (2023a,b) also found a mild (~0.1 dex) [Zn/Fe] enhancement in NGC 288 relative to NGC 362. Furthermore, the differences detected in

Table 1. Results of the isochrone fitting for NGC 6218, NGC 6362 (from this work) and NGC 288 (from Paper II).

Name	[M/H] (dex)	$E(B-V)$ (mag)	$(m-M)_0$ (mag)	Age (Gyr)
NGC 6218	$-1.17^{+0.05}_{-0.02}$	$0.20^{+0.01}_{-0.01}$	$13.57^{+0.01}_{-0.02}$	$13.42^{+0.38}_{-0.40}$
NGC 6362	$-0.92^{+0.02}_{-0.02}$	$0.07^{+0.01}_{-0.01}$	$14.43^{+0.01}_{-0.01}$	$13.86^{+0.33}_{-0.36}$
NGC 288	$-1.12^{+0.08}_{-0.08}$	$0.02^{+0.01}_{-0.01}$	$14.77^{+0.01}_{-0.01}$	$13.75^{+0.28}_{-0.22}$

Notes. The CMD fits and corner plots are shown in Figs. 1 and 2. All results obtained from the CARMA project can be found at: https://www.oas.inaf.it/en/research/m2-en/carma-en/

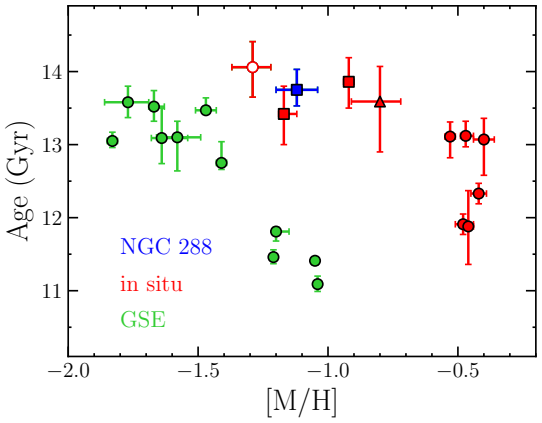

Fig. 3. Age-metallicity plane for all the GCs studied so far in the CARMA project. We plot the results for NGC 6218 and 6362 from this work as red filled squares. The position of NGC 288 from Paper II is highlighted as a blue filled square. Red and green filled circles represent in situ and GSE GCs from Paper I and Paper II, respectively, while the red empty circle is NGC 6205. The red filled triangle is ESO452-11 from Massari et al. (2025).

Table 2. Average chemical abundance ratios for NGC 288.

Element	NGC 288 (dex)
⟨[Fe/H]⟩	−1.21 ± 0.01 (0.03)
⟨[Mg/Fe]⟩	0.42 ± 0.02 (0.05)
⟨[Si/Fe]⟩	0.27 ± 0.01 (0.03)
⟨[Ca/Fe]⟩	0.31 ± 0.02 (0.07)
⟨[Ti/Fe]⟩	0.32 ± 0.02 (0.06)
⟨[Zn/Fe]⟩	−0.09 ± 0.02 (0.08)
⟨[YII/Fe]⟩	0.16 ± 0.04 (0.11)
⟨[BaII/Fe]⟩	0.35 ± 0.03 (0.08)
⟨[LaII/Fe]⟩	0.21 ± 0.01 (0.02)
⟨[EuII/Fe]⟩	0.39 ± 0.02 (0.06)

Notes. The standard deviation is reported in parenthesis.

the α- and neutron capture elements in NGC 288 and the in situ GC NGC 6218 are in agreement with those reported by Carretta et al. (2009); Carretta et al. (2010); Horta et al. (2020); Schiappacasse-Ulloa et al. (2024).

Finally, we find that the [EuII/Fe] of NGC 288 falls in between the GSE and in situ groups, in agreement with literature results (Shetrone & Keane 2000; Monty et al. 2024; Schiappacasse-Ulloa et al. 2025). However, since Eu is synthesized in various rare stellar events (e.g., magneto-rotational supernovae, collapsars, neutron star mergers, see Cescutti et al. 2015; Mösta et al. 2018; Siegel et al. 2019), its abundance is known to show significant intrinsic scatter, even among populations formed in the same environment (see e.g. Venn et al. 2012; Hill et al. 2019; Matsuno et al. 2021; Ou et al. 2024). As shown in the right panel of Fig. 4, the chemical spaces where the consistency between NGC 288 and in situ GCs is more remarkable are those relative to Eu. It has been well-established that the [EuII/X] ratios are a powerful tool to discriminate between in situ and accreted GCs due to the different sites and timescales of production of this species compared to the α-elements and to the light and heavy s-process elements (Kobayashi et al. 2020; Molero et al. 2023; Ou et al. 2024). Indeed, chemical evolutionary models predict that a more massive galaxy, such as the MW compared to GSE, would be expected to have lower values of Eu compared to these chemical elements that are due to either a higher star formation efficiency or the reduced impact of delayed r-process sources, such as neutron star mergers (Côté et al. 2019; Palla et al. 2025). We find that NGC 288 is depleted in all [EuII/X] ratios compared to GSE GCs and always shows compatible values with in situ GCs from C24. The relative differences between these two groups are consistent with those observed for either GCs and field stars (Fishlock et al. 2017; Aguado et al. 2021; Monty et al. 2024; Ou et al. 2024; Schiappacasse-Ulloa et al. 2025). This comparison demonstrates that the conditions of the gas where these clusters formed were extremely similar and coherent with the expectations for a galaxy like the MW in its earliest phases.

4. Discussion and conclusion

The picture that arises after combining all of these properties clearly suggests an in situ formation for NGC 288, which is at odds with its dynamical properties. Yet, just because these contradictory features have been determined in an extremely precise way, we can put forward a scenario that can accommodate all the observational evidences in a coherent picture.

In fact, we suggest that NGC 288 originally formed in situ within the MW, likely on a near-circular orbit with a low vertical height (Pfeffer et al. 2020), until the merger with GSE took place. It is well established that this interaction likely dynamically heated up the pre-existing MW disc, driving stars onto more eccentric orbits (Helmi et al. 2018; Di Matteo et al. 2019), a process commonly depicted as the Splash event (Belokurov et al. 2020). In Fig. 5, we compare the position of NGC 288 (blue filled square) with that of NGC 6218 and NGC 6362 (red filled squares) in the V_ϕ – [Fe/H] diagram, together with that of in situ stars[2] selected by Bellazzini et al. (2024). As depicted in this

[2] We note that NGC 288, NGC 6218, and NGC 6362 meet the selection criteria defined by these authors.

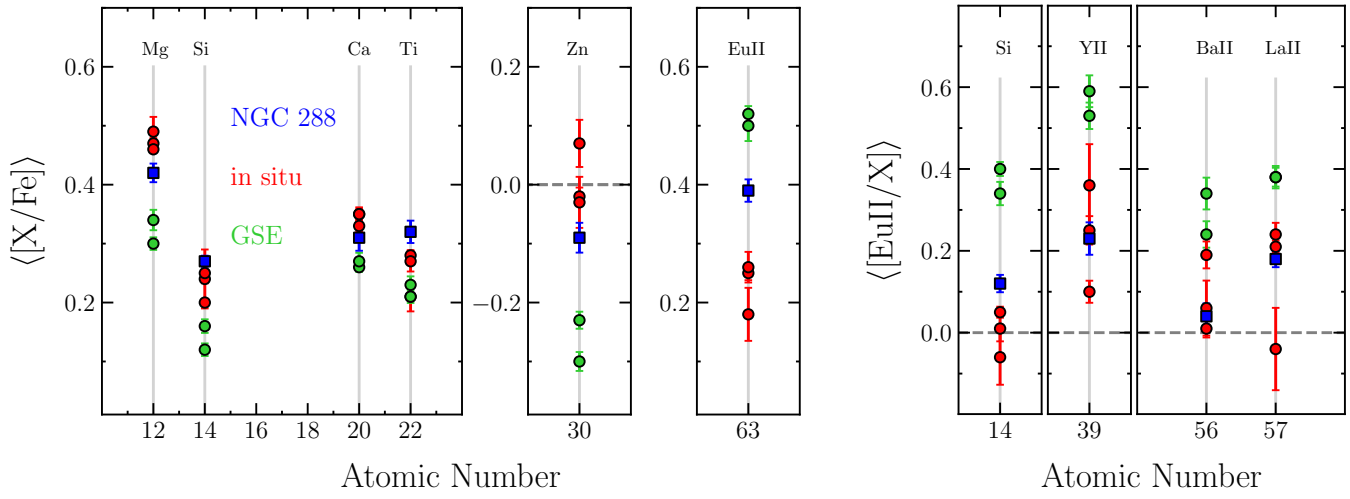

Fig. 4. Left panel: difference of mean abundance ratios of the α-elements [Mg/Fe], [Si/Fe], [Ca/Fe], [Ti/Fe], [Zn/Fe], and [EuII/Fe] between NGC 288 and GCs analyzed in C24. GCs are color coded according to their progenitors as in Fig. 3. Right panel: comparison of mean abundance ratios of EuII relative to other chemical elements (i.e. Si, YII, BaII, and LaII). Standard errors associated with the mean abundances are also reported.

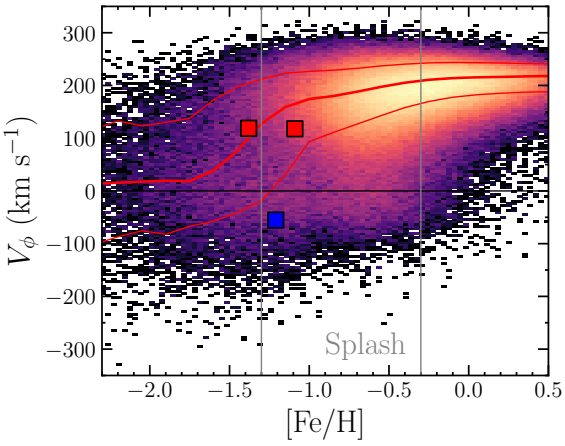

Fig. 5. Position of the NGC 288 (blue filled square) and the two in situ GCs (red filled squares) in the V_ϕ – [Fe/H] plane. In background we show the distribution of likely in situ stars from Bellazzini et al. (2024). The central red line highlights the median of the V_ϕ distribution, while the upper and lower lines trace the 16th and 84th percentiles, respectively. The grey vertical lines represent the upper and lower limits of the metallicity distribution function of Splash stars.

figure, NGC 6218 and NGC 6362 follow the distribution of in situ MW stars and GCs (Belokurov & Kravtsov 2024), likely forming during the rapid spin-up of the MW disc (Belokurov & Kravtsov 2022). On the contrary, NGC 288 display a V_ϕ value that is consistent with that of stars in the metal-poor tail of the Splash at [Fe/H] ~ -1.2 dex. Our interpretation is further reinforced by the chemical properties of Splash stars, whose abundances of the α-element are enhanced at about [α/Fe] = 0.3 dex (Belokurov et al. 2020), consistent with values measured for NGC 288. The fact that not all in situ GCs experienced similar dynamical perturbations from the GSE merger suggests that their initial spatial distribution within the Galaxy played a role in determining their response to this event. For example, the current larger apocentre in the orbit of NGC 288 suggests the possibility that this cluster could have already been located at a greater Galactocentric radius, compared to NGC 6218 and NGC 6362, making it more susceptible to the dynamical perturbations induced by the GSE merger. The idea that a major merger can similarly perturb the orbit of a GC has been supported also by cosmological simulations, which show that such events partially modify the kinematic distributions of in situ GCs (Keller et al. 2020; Chen & Gnedin 2022). In particular, mergers can displace a non-negligible fraction of these clusters from the Galactic disc to the halo by increasing their orbital eccentricity and energy (Li & Gnedin 2019; Trujillo-Gomez et al. 2021). Indeed, some old and metal-poor in situ GCs are expected to be found in the high energy and retrograde end of the $E - L_z$ plane (Pfeffer et al. 2020). Thus, this study may provide the first observational evidence of such a dynamical effect on an in situ MW GC, making NGC 288 the first example of a Splashed GC. In conclusion, these results mark NGC 288 as the first GC found to be dynamically consistent with an accreted progenitor, but yet not formed within it, demonstrating the effectiveness of combining homogeneous ages and chemical abundances and opening new avenues for understanding how GCs formed and evolved within our galaxy.

Acknowledgements. Based on observations collected at the ESO-VLT under the program 073.D-0211 (PI: E. Carretta). This work has made use of data from the European Space Agency (ESA) mission *Gaia* https://www.cosmos.esa.int/gaia), processed by the *Gaia* Data Processing and Analysis Consortium (DPAC, https://www.cosmos.esa.int/web/gaia/dpac/consortium). Funding for the DPAC has been provided by national institutions, in particular the institutions participating in the *Gaia* Multilateral Agreement. E.C. is grateful to M. Bellazzini and A. Della Croce for useful discussions, comments and support to this work. This research is funded by the project *LEGO – Reconstructing the building blocks of the Galaxy by chemical tagging* (PI: A. Mucciarelli), granted by the Italian MUR through contract PRIN 2022LLP8TK_001. E.C. and D.M. acknowledge the support to this study by the PRIN INAF 2023 grant ObFu *CHAM – Chemodynamics of the Accreted Halo of the Milky Way* (PI: M. Bellazzini). D.M. acknowledges financial support from PRIN-MIUR-22: CHRONOS: adjusting the clock(s) to unveil the CHRONO-chemo-dynamical Structure of the Galaxy" (PI: S. Cassisi) granted by the European Union - Next Generation EU. D.M. acknowledges the support to activities related to the ESA/*Gaia* mission by the Italian Space Agency (ASI) through contract 2018-24-HH.0 and its addendum 2018-24-HH.1-2022 to the National Institute for Astrophysics (INAF). Co-funded by the European Union (ERC-2022-AdG, "StarDance: the non-canonical evolution of stars in clusters",

Grant Agreement 101093572, PI: E. Pancino). Views and opinions expressed are however those of the author(s) only and do not necessarily reflect those of the European Union or the European Research Council. Neither the European Union nor the granting authority can be held responsible for them. M.M. acknowledges support from the Agencia Estatal de Investigación del Ministerio de Ciencia e Innovación (MCIN/AEI) under the grant "RR Lyrae stars, a lighthouse to distant galaxies and early galaxy evolution" and the European Regional Development Fund (ERDF) with reference PID2021-127042OB-I00.

References

Aguado, D. S., Belokurov, V., Myeong, G. C., et al. 2021, ApJ, 908, L8
Aguado-Agelet, F., Massari, D., Monelli, M., et al. 2025, A&A, 704, A255
Andrae, R., Fouesneau, M., Creevey, O., et al. 2018, A&A, 616, A8
Baumgardt, H., & Vasiliev, E. 2021, MNRAS, 505, 5957
Bellazzini, M., Pecci, F. F., Ferraro, F. R., et al. 2001, AJ, 122, 2569
Bellazzini, M., Ibata, R., Malhan, K., et al. 2020, A&A, 636, A107
Bellazzini, M., Massari, D., Ceccarelli, E., et al. 2024, A&A, 683, A136
Belokurov, V., & Kravtsov, A. 2022, MNRAS, 514, 689
Belokurov, V., & Kravtsov, A. 2024, MNRAS, 528, 3198
Belokurov, V., Erkal, D., Evans, N. W., Koposov, S. E., & Deason, A. J. 2018, MNRAS, 478, 611
Belokurov, V., Sanders, J. L., Fattahi, A., et al. 2020, MNRAS, 494, 3880
Callingham, T. M., Cautun, M., Deason, A. J., et al. 2022, MNRAS, 513, 4107
Cardelli, J. A., Clayton, G. C., & Mathis, J. S. 1989, ApJ, 345, 245
Carretta, E., Bragaglia, A., Gratton, R., & Lucatello, S. 2009, A&A, 505, 139
Carretta, E., Bragaglia, A., Gratton, R., et al. 2010, ApJ, 712, L21
Carretta, E., Bragaglia, A., Gratton, R. G., et al. 2013, A&A, 557, A138
Cassisi, S., Salaris, M., Castelli, F., & Pietrinferni, A. 2004, ApJ, 616, 498
Castelli, F., & Kurucz, R. L. 2003, IAU Symp., 210, A20
Ceccarelli, E., Mucciarelli, A., Massari, D., Bellazzini, M., & Matsuno, T. 2024, A&A, 691, A226
Cescutti, G., Romano, D., Matteucci, F., Chiappini, C., & Hirschi, R. 2015, A&A, 577, A139
Chen, Y., & Gnedin, O. Y. 2022, MNRAS, 514, 4736
Chen, Y., & Gnedin, O. Y. 2024, Open J. Astrophys., 7, 23
Côté, B., Eichler, M., Arcones, A., et al. 2019, ApJ, 875, 106
Di Matteo, P., Haywood, M., Lehnert, M. D., et al. 2019, A&A, 632, A4
Dotter, A., Sarajedini, A., Anderson, J., et al. 2010, ApJ, 708, 698
Fishlock, C. K., Yong, D., Karakas, A. I., et al. 2017, MNRAS, 466, 4672
Forbes, D. A. 2020, MNRAS, 493, 847
Forbes, D. A., & Bridges, T. 2010, MNRAS, 404, 1203
Gaia Collaboration (Prusti, T., et al.) 2016, A&A, 595, A1
Gaia Collaboration (Babusiaux, C., et al.) 2018, A&A, 616, A10
Gaia Collaboration (Vallenari, A., et al.) 2023, A&A, 674, A1
Gallart, C., Bernard, E. J., Brook, C. B., et al. 2019, Nat. Astron., 3, 932
Gontcharov, G. A., Khovritchev, M. Y., Mosenkov, A. V., et al. 2021, MNRAS, 508, 2688
González-Koda, Y. K., Ruiz-Lara, T., Gallart, C., et al. 2025, A&A, 704, A259
Green, E. M., & Norris, J. E. 1990, ApJ, 353, L17
Grevesse, N., & Sauval, A. J. 1998, Space Sci. Rev., 85, 161
Harris, W. E. 2010, arXiv e-prints [arXiv:1012.3224]
Helmi, A. 2020, ARA&A, 58, 205
Helmi, A., Babusiaux, C., Koppelman, H. H., et al. 2018, Nature, 563, 85
Hidalgo, S. L., Pietrinferni, A., Cassisi, S., et al. 2018, ApJ, 856, 125
Hill, V., Skúladóttir, Á., Tolstoy, E., et al. 2019, A&A, 626, A15
Horta, D., Schiavon, R. P., Mackereth, J. T., et al. 2020, MNRAS, 493, 3363
Keller, B. W., Kruijssen, J. M. D., Pfeffer, J., et al. 2020, MNRAS, 495, 4248
Kobayashi, C., Karakas, A. I., & Lugaro, M. 2020, ApJ, 900, 179
Kruijssen, J. M. D., Pfeffer, J. L., Reina-Campos, M., Crain, R. A., & Bastian, N. 2019, MNRAS, 486, 3180
Kurucz, R. L. 2005, Memorie della Societa Astronomica Italiana Supplementi, 8, 14
Leaman, R., VandenBerg, D. A., & Mendel, J. T. 2013, MNRAS, 436, 122
Li, H., & Gnedin, O. Y. 2019, MNRAS, 486, 4030
Malhan, K., Ibata, R. A., Sharma, S., et al. 2022, ApJ, 926, 107
Marín-Franch, A., Aparicio, A., Piotto, G., et al. 2009, ApJ, 694, 1498
Massari, D., Mucciarelli, A., Dalessandro, E., et al. 2017, MNRAS, 468, 1249
Massari, D., Koppelman, H. H., & Helmi, A. 2019, A&A, 630, L4
Massari, D., Aguado-Agelet, F., Monelli, M., et al. 2023, A&A, 680, A20
Massari, D., Bellazzini, M., Libralato, M., et al. 2025, A&A, 698, A197
Matsuno, T., Hirai, Y., Tarumi, Y., et al. 2021, A&A, 650, A110
Milone, A. P., Piotto, G., Bedin, L. R., et al. 2012, A&A, 540, A16
Molero, M., Magrini, L., Matteucci, F., et al. 2023, MNRAS, 523, 2974
Monty, S., Yong, D., Marino, A. F., et al. 2023a, MNRAS, 518, 965
Monty, S., Yong, D., Massari, D., et al. 2023b, MNRAS, 522, 4404
Monty, S., Belokurov, V., Sanders, J. L., et al. 2024, MNRAS, 533, 2420
Mori, A., Di Matteo, P., Salvadori, S., et al. 2024, A&A, 690, A136
Mösta, P., Roberts, L. F., Halevi, G., et al. 2018, ApJ, 864, 171
Mucciarelli, A. 2013, arXiv e-prints [arXiv:1311.1403]
Mucciarelli, A., Pancino, E., Lovisi, L., Ferraro, F. R., & Lapenna, E. 2013, ApJ, 766, 78
Mucciarelli, A., Bellazzini, M., & Massari, D. 2021, A&A, 653, A90
Nardiello, D., Libralato, M., Piotto, G., et al. 2018, MNRAS, 481, 3382
Ou, X., Ji, A. P., Frebel, A., Naidu, R. P., & Limberg, G. 2024, ApJ, 974, 232
Pagnini, G., Di Matteo, P., Khoperskov, S., et al. 2023, A&A, 673, A86
Palla, M., Molero, M., Romano, D., & Mucciarelli, A. 2025, A&A, 699, A209
Pasquini, L., Avila, G., Blecha, A., et al. 2002, The Messenger, 110, 1
Peñarrubia, J., Walker, M. G., & Gilmore, G. 2009, MNRAS, 399, 1275
Pfeffer, J. L., Trujillo-Gomez, S., Kruijssen, J. M. D., et al. 2020, MNRAS, 499, 4863
Piotto, G., Milone, A. P., Bedin, L. R., et al. 2015, AJ, 149, 91
Salaris, M., Chieffi, A., & Straniero, O. 1993, ApJ, 414, 580
Sarajedini, A., & Demarque, P. 1990, ApJ, 365, 219
Schiappacasse-Ulloa, J., Lucatello, S., Cescutti, G., & Carretta, E. 2024, A&A, 685, A10
Schiappacasse-Ulloa, J., Magrini, L., Lucatello, S., et al. 2025, A&A, 699, A41
Shetrone, M. D., & Keane, M. J. 2000, AJ, 119, 840
Siegel, D. M., Barnes, J., & Metzger, B. D. 2019, Nature, 569, 241
Souza, S. O., Libralato, M., Nardiello, D., et al. 2024, A&A, 690, A37
Stetson, P. B., & Pancino, E. 2008, PASP, 120, 1332
Stetson, P. B., Vandenberg, D. A., & Bolte, M. 1996, PASP, 108, 560
Trujillo-Gomez, S., Kruijssen, J. M. D., Reina-Campos, M., et al. 2021, MNRAS, 503, 31
VandenBerg, D. A., Brogaard, K., Leaman, R., & Casagrande, L. 2013, ApJ, 775, 134
Vasiliev, E., & Baumgardt, H. 2021, MNRAS, 505, 5978
Venn, K. A., Shetrone, M. D., Irwin, M. J., et al. 2012, ApJ, 751, 102
White, S. D. M., & Frenk, C. S. 1991, ApJ, 379, 52

Appendix A: Age measurement

A.1. Differential reddening correction

To ensure the highest quality data for the fitting process, we applied a differential reddening correction to the HST photometry of NGC 6218 and NGC 6362 following the approach described by Milone et al. (2012), after selecting for proper-motion based membership ($p > 90\%$). We used RGB stars to define the reference sample, as their lower photometric errors make them preferable over main sequence stars, despite their smaller number. The differential reddening value ($\Delta E(B-V)$) associated with each star was derived as the median offset from the RGB mean ridge line, defined in a CMD oriented along the reddening vector, based on the 30 nearest reference stars. We employed the Cardelli et al. (1989) extinction law, adopting $R_V = 3.1$. This iterative process was repeated for each star until the residual $\Delta E(B-V)$ matched the typical photometric error, reaching convergence after two iterations. The effect of the differential reddening corrections on the CMD of NGC 6362 is illustrated in Fig. A.1, and the corresponding reddening map is displayed in Fig. A.2.

A.2. Isochrone fitting

The age of NGC 6218 and NGC 6362 were estimated using the method described in Paper I. We employed isochrones from the BaSTI library (Hidalgo et al. 2018) spanning the age range from 6 to 15 Gyr and the [M/H] range from -2.5 to 0.0 dex (in steps of 0.1 Gyr and 0.01 dex, respectively). The CARMA isochrone fitting code was executed assuming Gaussian priors on the metallicity (solar-scaled models), color excess, and distance modulus centred on values provided in Harris (2010), with dispersions of 0.1, 0.05 and 0.1, respectively. We recall that the use of solar-scaled models was deliberately chosen to avoid imposing assumptions about the α-element abundance. On top of this, we chose to use photometric data in optical bands, where the equivalence between solar-scaled and α-enhanced models at the same global metallicity has been robustly demonstrated (e.g. Salaris et al. 1993; Cassisi et al. 2004). The code was ran on both the (m_{F814W}, $m_{F606W} - m_{F814W}$) CMD and the (m_{F606W}, $m_{F606W} - m_{F814W}$) CMD. In Table 1 we report the average value of the two runs and the associated asymmetric uncertainties calculated in order to enclose both the upper and lower limits of each run.

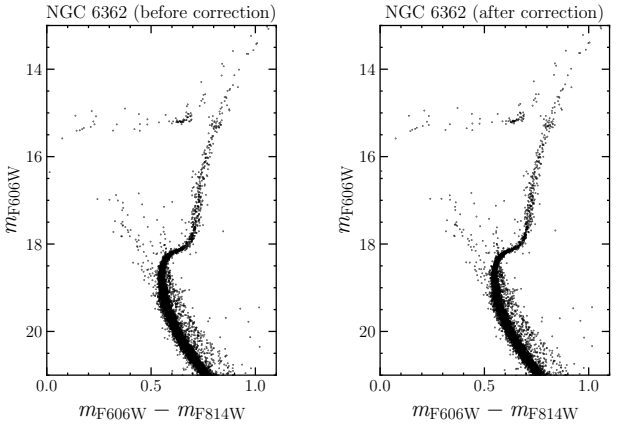

Fig. A.1. Comparison of the CMDs of NGC 6362 before (left panel) and after (right panel) correcting for the effect of differential reddening.

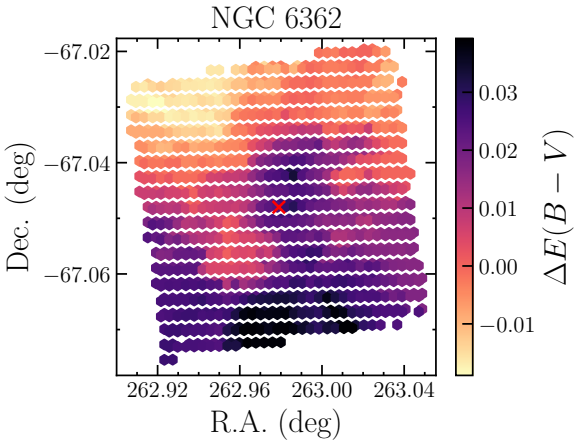

Fig. A.2. Differential reddening map for the GC NGC 6362. The red cross indicates the centre of the cluster (Vasiliev & Baumgardt 2021).

Appendix B: Chemical analysis

B.1. Stellar parameters

We derived the effective temperature (T_{eff}) and the surface gravity (log g) using the *Gaia* Data Release 3 (Gaia Collaboration 2023) photometric dataset exploiting the $(BP-RP)_0$ - T_{eff} relation provided by Mucciarelli et al. (2021). We assumed a color excess $E(B-V)$ from the Harris (2010) catalogue and followed the iterative prescription described in Gaia Collaboration (2018) to efficiently remove the effects of the extinction on the observed (BP – RP) color. Internal errors in T_{eff} stem from the propagation of the uncertainties in the photometry, reddening and assumed color - T_{eff} relation and they are of the order of 80 - 100 K. Surface gravities (log g) have been estimated from the Stefan-Boltzmann relation, assuming the photometric T_{eff} and a stellar mass of 0.8 $M_\odot$, the G-band bolometric corrections provided by Andrae et al. (2018), and a distance of 8.99 ± 0.09 kpc (Baumgardt & Vasiliev 2021), consistent with the procedure described in C24. We note that the distance by Baumgardt & Vasiliev (2021) is fully consistent with that derived in Paper II. We assume a conservative estimate of the uncertainty on the surface gravity of 0.1 dex. In the end, we calculated microturbulent velocities (v_t) by erasing any trend between the measured iron abundances and reduced equivalent widths. Uncertainties on v_t are typically lower than 0.2 km s^{-1}. All the atmospheric parameters are listed in Table B.1.

B.2. Derivation of abundances

We employed `ATLAS9` (Kurucz 2005) model atmospheres computed under the assumptions of plane-parallel geometry, hydrostatic and radiative equilibrium, and local thermodynamic equilibrium for all the chemical elements, starting from an α-enhanced model. Chemical abundances of Mg, Si, Ca, Ti, and Zn were obtained comparing theoretical and observed equivalent widths (EWs), measured with the code `DAOSPEC` (Stetson & Pancino 2008) exploiting the tool `4DAO` (Mucciarelli 2013), using the code `GALA` (Mucciarelli et al. 2013). Atomic lines for the

Table B.1. Information on the targets.

Star ID	ID Gaia DR3	$T_{\rm eff}$ (K)	log g (dex)	$v_{\rm t}$ (km s^{-1})
200011	2342906141734490880	4486	1.32	1.4
200055	2342907825361664128	4844	2.00	1.5
200050	2342903083717827200	4823	1.96	1.4
200004	2342903118077555840	4242	0.87	1.5
200002	2342903045061492224	4093	0.65	1.5
200009	2342907580546992128	4458	1.24	1.5
200038	2342903045061492224	4745	1.78	1.4
200021	2342904698625661824	4616	1.53	1.4
200061	2342908340757896704	4908	2.08	1.4
200020	2342904423747772416	4597	1.49	1.4

Notes. We list the star ID from previous literature works (e.g. Carretta et al. 2009), ID from *Gaia* DR3, effective temperature, surface gravity, and microturbulent velocity. Typical uncertainties are of the order of 100 K, 0.01 dex, and 0.2 km s^{-1} for $T_{\rm eff}$, log g, and $v_{\rm t}$ respectively.

Table B.2. Iron and α-elements abundances for target stars in NGC 288.

Star ID	[Fe/H] (dex)	[Mg/Fe] (dex)	[Si/Fe] (dex)	[Ca/Fe] (dex)	[Ti/Fe] (dex)
200011	-1.19 ± 0.09	0.49 ± 0.04	0.29 ± 0.10	0.34 ± 0.05	0.33 ± 0.09
200055	-1.15 ± 0.11	0.38 ± 0.03	0.25 ± 0.10	0.19 ± 0.04	0.24 ± 0.05
200050	-1.21 ± 0.10	0.44 ± 0.02	0.28 ± 0.09	0.40 ± 0.06	0.28 ± 0.06
200004	-1.26 ± 0.07	-	0.27 ± 0.11	0.41 ± 0.07	0.42 ± 0.13
200002	-1.26 ± 0.06	-	0.32 ± 0.12	0.40 ± 0.10	0.43 ± 0.15
200009	-1.22 ± 0.10	0.45 ± 0.04	0.22 ± 0.12	0.29 ± 0.05	0.33 ± 0.09
200038	-1.17 ± 0.11	0.40 ± 0.04	0.26 ± 0.10	0.27 ± 0.04	0.28 ± 0.06
200021	-1.21 ± 0.10	0.43 ± 0.03	0.25 ± 0.10	0.30 ± 0.05	0.32 ± 0.07
200061	-1.22 ± 0.10	0.33 ± 0.03	0.28 ± 0.08	0.23 ± 0.05	0.26 ± 0.05
200020	-1.21 ± 0.10	0.43 ± 0.03	0.27 ± 0.10	0.26 ± 0.04	0.29 ± 0.08

Table B.3. Same as Table B.2, but for Zn, YII, BaII, LaII, and EuII.

Star ID	[Zn/Fe] (dex)	[YII/Fe] (dex)	[BaII/Fe] (dex)	[LaII/Fe] (dex)	[EuII/Fe] (dex)
200011	-0.09 ± 0.16	0.38 ± 0.15	0.49 ± 0.17	0.20 ± 0.05	0.43 ± 0.05
200055	-0.03 ± 0.14	-0.01 ± 0.15	0.17 ± 0.17	0.21 ± 0.05	0.35 ± 0.06
200050	-0.06 ± 0.13	0.15 ± 0.14	0.39 ± 0.16	0.17 ± 0.05	0.37 ± 0.06
200004	-0.21 ± 0.15	0.19 ± 0.15	0.32 ± 0.15	0.20 ± 0.05	0.40 ± 0.05
200002	-0.24 ± 0.14	0.31 ± 0.15	0.37 ± 0.16	0.22 ± 0.05	0.47 ± 0.05
200009	-0.06 ± 0.16	0.10 ± 0.15	0.27 ± 0.16	0.20 ± 0.05	0.36 ± 0.05
200038	0.02 ± 0.14	0.04 ± 0.13	0.31 ± 0.15	0.22 ± 0.05	0.40 ± 0.06
200021	-0.08 ± 0.15	0.10 ± 0.15	0.35 ± 0.16	0.21 ± 0.04	0.46 ± 0.05
200061	-0.01 ± 0.14	0.15 ± 0.14	0.39 ± 0.15	0.26 ± 0.06	0.28 ± 0.06
200020	-0.13 ± 0.15	0.22 ± 0.15	0.39 ± 0.16	0.18 ± 0.05	0.34 ± 0.05

chemical elements that have saturated hyperfine/isotopic splitting transitions (YII, BaII, LaII, and EuII) were analysed through spectral synthesis using the proprietary code SALVADOR.

The final abundance ratios are scaled to the solar values provided by Grevesse & Sauval (1998), that is the solar composition assumed when computing ATLAS9 model atmospheres (Castelli & Kurucz 2003). We report chemical abundances for the 10 RGB stars analysed in this work in Tables B.2 and B.3.

The errors on the abundance ratios have been estimated as the squared sum of two components (see C24 for a complete discussion): (i) internal errors due to the EW measurement and (ii) errors arising from the computation of atmospheric parameters. Thus, the uncertainties have been estimated as

$$\sigma_{\rm [Fe/H]} = \sqrt{\frac{\sigma_{Fe}^2}{N_{Fe}} + (\delta_{Fe}^{T_{\rm eff}})^2 + (\delta_{Fe}^{\log g})^2 + (\delta_{Fe}^{v_{\rm t}})^2},$$

$$\sigma_{\rm [X/Fe]} = \sqrt{\frac{\sigma_X^2}{N_X} + \frac{\sigma_{Fe}^2}{N_{Fe}} + (\delta_X^{T_{\rm eff}} - \delta_{Fe}^{T_{\rm eff}})^2 + (\delta_X^{\log g} - \delta_{Fe}^{\log g})^2 + (\delta_X^{v_{\rm t}} - \delta_{Fe}^{v_{\rm t}})^2},$$

where $\sigma_{X,Fe}$ is the dispersion around the mean of chemical abundances, $N_{X,Fe}$ is the number of used lines and $\delta_{X,Fe}^{i}$ are the abundance differences obtained by varying the parameter i.